Antiferromagnetic fluctuations and charge carrier localization in ferromagnetic bilayer manganites: electrical resistivity scales exponentially with short-range order controlled by temperature and magnetic field

T G Perring, D T Adroja, J D M Champion, G Aeppli, G Chaboussant, T Kimura, Y Tokura, P Manuel

Antiferromagnetic fluctuations and charge carrier localization in ferromagnetic bilayer manganites: electrical resistivity scales exponentially with short-range order controlled by temperature and magnetic field

T. G. Perring[1], D. T. Adroja[1], J. D. M. Champion[1], G. Aeppli [2,3,4], G. Chaboussant[5], T. Kimura[6] , Y. Tokura[7,8,9] , and P. Manuel[1]

[1] ISIS Neutron and Muon Source, STFC Rutherford Appleton Laboratory, Didcot, Oxon OX11 0QX, UK.
[2] Physics Department, ETH CH-8093 Zurich, Switzerland
[3] Institut de Physique, EPFL CH-1015 Lausanne, Switzerland
[4] Paul Scherrer Institut, Swiss Light Source, CH-5232 Villigen PSI, Switzerland
[5] Laboratoire Léon Brillouin, CEA, CNRS, Université Paris-Saclay, CEA Saclay, 91191 Gif-sur-Yvette, France
[6] Department of Advanced Materials Science, University of Tokyo, Kashiwa, Chiba 277-8561, Japan
[7]Department of Applied Physics, University of Tokyo, Tokyo 113-8656, Japan.
[8] RIKEN Center for Emergent Matter Science (CEMS), Wako 351-0198, Japan
[9] Tokyo College, University of Tokyo, Tokyo 113-8656, Japan

Abstract. The compound $La_{2-2x}Sr_{1+2x}Mn_2O_7$, $x = 0.30 – 0.40$, consists of bilayers of ferromagnetic metallic MnO_2 sheets that are separated by insulating layers. The materials show colossal magnetoresistance – a reduction in resistivity of up to two orders of magnitude in a field of 7 T – at their three-dimensional ordering temperatures, $T_C = 90$ K – 126 K, and are the layered analogues of the widely studied pseudo-cubic perovskite manganites, $R_{1-x}A_xMnO_3$ (R = rare earth, A = Ca, Sr, Ba, Pb). Two distinct short-range orderings – antiferromagnetic fluctuations and correlated polarons, which are related to the magnetic and the lattice degrees of freedom respectively – have previously been discovered in $La_{2-2x}Sr_{1+2x}Mn_2O_7$, $x = 0.40$, and have each been qualitatively connected to the resistivity. Here, in a comprehensive study as a function of both temperature and magnetic field for the

different hole-concentrations per Mn site of $x = 0.30$ and 0.35, we show that antiferromagnetic fluctuations also appear at temperatures just above T_C, and that the intensities of both the antiferromagnetic fluctuations and polaron correlations closely track the resistivity. In particular, for $x = 0.35$ we show that there is a simple scaling relation between the intensities of the antiferromagnetic fluctuations and the in-plane resistivity that applies for the temperatures and magnetic fields used in the experiments. The results show that antiferromagnetic fluctuations are a common feature of $La_{2-2x}Sr_{1+2x}Mn_2O_7$ with ferromagnetic bilayers, and that there is a close connection between the antiferromagnetic fluctuations and polarons in these materials.

1. Introduction

1.1 Roger Cowley and magnetic phase transitions

Throughout a wide-ranging career, a long-standing interest of Roger Cowley was phase transitions in magnetic materials. From the very start of his career, he had made seminal contributions in the field of structural phase transitions, for example testing the idea that a soft phonon mode is responsible for the phase transition in a certain perovskite [1]. His seminal work on magnetic phase transitions included a series of papers concerning the percolation transition in Ising and Heisenberg insulators diluted with magnetic and non-magnetic impurities, and the random field Ising model [2-6].

He was a master of neutron scattering, which is the premier technique to probe the spatial and temporal dynamics of magnetic systems at the scales set by the atomic spacing and the magnetic interactions strengths. The scattering process itself directly yields the wave-vector and frequency spectrum of the two-spin correlation function, barring simple and well-understood constants and geometric terms, and so cuts straight to the underlying physics and enables the most exacting quantitative tests of theories of order parameter fluctuations and phase transitions.

His classic experiments on soft modes and random field effects in diluted magnets were performed on the reactor-based triple axis spectrometer (TAS), which with its flexible control of resolution and more or less unrestricted access to the four dimensional (vector momentum and energy) phase space relevant for many problems in condensed matter physics, permitted, during most of his lifetime, the most precise exploration of dynamics in the ordered state and

of critical phenomena. However, he was quick to see the opportunities of time-of-flight methods at the pulsed source ISIS in the UK. Spectrometers at such sources require a very different approach to experiments: they have a large solid angle of detectors that map the wave vector and frequency dependence of the correlations in parallel, rather than point-by-point as on a TAS, and the required experimental skills have as much to do with the adroit use of software to explore the large data sets collected on the instruments as they do with mastery of the hardware. One of the earliest experiments that did much to establish the new time-of-flight approach to the exploration of dynamics in single crystals was Roger Cowley's influential work (with Alan Tennant and Stephen Nagler) that unambiguously showed the fractionalisation of spin excitations in the one-dimensional Heisenberg antiferromagnetic chain [7].

1.2 Bilayer manganites

This article concerns the existence of antiferromagnetic correlations and polaron dynamics in the vicinity of the ferromagnetic phase transition in (poorly) metallic manganites. Two connections with ideas in the section above are as follows: the character of the magnetic dynamics changing through a phase transition, and also that the original discovery of an unexpected phenomenon – the appearance of ***antiferromagnetic*** fluctuations at a ***ferromagnetic*** transition – was serendipitous and only possible because of the parallel mapping of the dynamics in a large detector array that included regions of reciprocal space that were originally of no interest.

The starting point to understand the physics of the manganites is the venerable double exchange model [8]. Each Mn ion has a local magnetic moment with spin S=3/2 arising from three electrons in the t_{2g} d-orbitals, and a fraction (1-x) of the Mn ions have a fourth electron in a higher energy e_g orbital, whose spin is aligned parallel to the local moment by strong Hund's rule coupling J_H~2eV. The essential physics is a competition between delocalisation of the e_g electrons, favouring a fully spin polarised ferromagnetic (FM) metal, and localisation, due to local lattice distortions around the Jahn-Teller active Mn^{3+} ions self-trapping the e_g electrons [9]. For sufficiently high hole concentration, x, the e_g electrons may form ordered lattices; the subsequent distortions of the MnO_6 octahedral units which make up the perovskite structure can favour occupancy of one e_g orbital over others, which in turn can

control the magnetic exchange between Mn ions. It is the delicate balance between delocalisation and localisation, together with the coupling of the magnetic, lattice, charge and orbital degrees of freedom that results in the sensitivity of the transport properties to external stimuli. These manifest themselves through insulator-metal transitions induced by electromagnetic perturbations (including photons) and strain fields [10-13]. Theoretical and experimental work considers phase segregation in the manganites, at length scales from 1 nm to O(μm) [14]. Transport measurements, neutron scattering and most spectacularly STM and AFM microscopy [15,16] reveal the coexistence of metallic and insulating phases for some manganites, where one phase shrinks or grows at the expense of others as temperature or magnetic field is altered.

Two discoveries salient to an understanding of the resistivity of the bilayer manganites $La_{2-2x}Sr_{1+2x}Mn_2O_7$, $x = 0.30 – 0.40$ [17, 18] (figure 1(a)) are those of antiferromagnetic (AF) fluctuations [19] and polaron correlations [20]. Short-range, short-lived AF correlations were observed [19] in the case of $x = 0.40$ to appear at (0.5,0,0) on warming through the three-dimensional ordering temperature $T_C = 126$K of this ferromagnet, decreasing in intensity with increasing temperature but surviving to at least 2.2 T_C, and coexisting with the conventional FM critical scattering. The intensity of the scattering qualitatively follows that of the resistivity. The correlation length was found to be only ~ 2 a, where a is the distance between adjacent Mn sites within the bilayers, but with lifetimes considerably longer than the timescales defined both by characteristic phonon frequencies associated with the MnO_6 breathing and stretching modes, and by the hopping integral $t \sim 0.3$ eV for movement of electrons between adjacent Mn ions. Within the spatial and temporal region defined by the correlation length and lifetime, the AF fluctuations break the long-range tetragonal symmetry, as they correspond to Mn moment reversal along only one of the in-plane Mn-Mn bonds (shown schematically in figure 1(b)). The significance of the long-lived AF fluctuations is that within the double-exchange model, adjacent Mn moments that are parallel provide a pathway for hopping of the e_g electrons, whereas antiparallel alignment blocks conduction. The latter follows from the penalty of the intrasite Hund's rule energy experienced by an e_g electron hopping to a Mn^{4+} site pointing in the opposite direction to the local t_{2g} moment. Soon after this discovery, diffuse x-ray scattering from a crystal of the same composition, $x = 0.40$ [20], revealed the presence of local lattice distortions around the Mn sites. Just like the AF fluctuations, they only appear in the paramagnetic, insulating phase above T_C, and persist with decreasing intensity to at least 2.6 T_C. The polarons exhibited

short-range order with a characteristic wavevector ($\pm\delta$, 0, $\pm$1) where $\delta \approx 0.3$, and the intensity of associated scattering followed a behaviour similar to that of the AF fluctuations as temperature was varied. Detailed investigations [21, 22] revealed the nature of the polaron correlations. The widths of the MnO_6 octahedra in both sheets of a bilayer are modulated along one of the Mn-Mn directions in the plane of the bilayer, with wavevector (δ, 0, 0). The octahedra are tilted by rotation about the other in-plane Mn-Mn direction with the same period, but in anti-phase. At $T = T_C + 13$ K, the correlation lengths are $\approx 6\ a$, $\approx 4\ a$ and $\sim c/2$ along the modulation wavevector, in the perpendicular in-plane direction, and perpendicular to the bilayers respectively. The same behaviour – correlated polarons with modulation vector (≈0.3, 0 0) whose scattering intensity broadly follows the resistivity – was reported for higher hole concentrations $x = 0.40 – 0.48$ [23]. Two unanswered questions are (i) are the AF fluctuations peculiar to the hole concentration $x = 0.40$, or do they exist for a range of x, and (ii) how are the two phenomena – AF fluctuations and correlated polarons –related. Here we answer both questions by showing comprehensive measurements of properties of both as a function of temperature and applied magnetic field for $x = 0.30$ and 0.35.

$La_{2-2x}Sr_{1+2x}Mn_2O_7$ crystals with $x = 0.30$ and 0.35 were chosen for the study for the following reasons. First, $x = 0.35$ has the same FM long-range order as $x = 0.40$, with very similar $T_C = 121$ K, and has the same qualitative behaviour of the in-plane, ρ_{ab}, and perpendicular resistivities, ρ_c. However, it lies well in the composition range ~0.32 – 0.40 for which the ground state is FM, and away from the range x ~0.40 – 0.48 for which the structure within the bilayers shows initially AF long-range ordering for $T < T_N$ then AF canted order for $T < T_C < T_N$ [24, 25]. The instance of $x = 0.35$ therefore provides an example free of complications arising from the proximity to phases with AF character in the ground state. Second, $x = 0.30$ has qualitatively different ρ_{ab}, compared to $x = 0.35$ and 0.40 (compare figures 2(b) and 3(b)). For both $x = 0.30$ and 0.35, ρ_c peaks at the three-dimensional ordering temperatures and shows colossal negative magnetoresistance near these temperatures. However, whereas ρ_{ab} ($x = 0.35$) has the same qualitative behaviour as ρ_c (albeit two orders of magnitude smaller, reflecting the insulating barriers in the layered structure), ρ_{ab} ($x = 0.30$) continues to increase to about 270 K. For $x = 0.30$, the magnetic structure within the bilayers is FM, just as for $x = 0.35$ and 0.40, but the bilayers are now coupled antiferromagnetically, with three-dimensional ordering temperature $T_N = 90$ K. The case of $x = 0.30$ provides a

qualitatively different material, as far as ~~of~~ resistivity and long-range magnetic ordering are concerned, for which to measure the development of the AF and polaron correlations.

2. Methods

Single crystals of $La_{2-2x}Sr_{1+2x}Mn_2O_7$, x = 0.30 and 0.35, were grown using the floating zone method as described before [17]. The AF and polaron correlations as a function of both temperature and applied magnetic field were studied by neutron scattering from single crystal samples with mass 2.9g (x=0.35) and 0.7g (x=0.30). Intensity maps for the AF correlations were collected as a function of temperature and magnetic field using the HET spectrometer at the ISIS Neutron and Muon Source at the STFC Rutherford Appleton Laboratory, UK, with an incident neutron energy of 20 meV. This instrument had detector arrays that enabled intensity maps to be collected as a function of energy simultaneously along the *(h, 0, 0)* and *(h, h, 0)* directions in the sheets of the bilayers, and which also allowed the AF fluctuations at (0.5, 0) to be isolated from scattering due to non-magnetic and sample environment scattering, as explained below. We collected data at three temperatures 6 K, 126 K and 300 K using the MAPS spectrometer at ISIS with an incident energy of 65 meV to give detailed intensity maps as a function of energy in the *(h, k, 0)* plane. The diffuse scattering arising from polaron correlations were measured on the PRISMA instrument at ISIS, operating in white beam (Laue) diffraction mode.

3. Results

Figures 1(c-f) show representative maps gathered in zero applied magnetic field from the single crystal with x = 0.35. In addition, figure 1(g) shows an overview of the energy-integrated magnetic scattering in the (h,k,0) plane at 126K, just above $T_C \equiv 121$ K, collected on the MAPS instrument. At integer h and k there is the ~~ferromagnetic~~ critical scattering that is expected for a ferromagnet, but at the AF wavevector (0.5, 0, 0) and symmetry related positions there is additional diffuse intensity. The magnetic origin is confirmed by the fact that the intensity at (0.5, 1, 0) and symmetry related positions, which arises at the same position in the Brillouin zone as (0.5, 0, 0), is weaker, whereas scattering from lattice fluctuations would be more intense. Figures 1(c) and 1(d) show spectra of the AF fluctuations

as a function of excitation energy, ε, and momentum along the *(h, 0, 0)* direction in the plane of the bilayers i.e. along one of the Mn-Mn bond directions. Figure 1(c) shows that the AF scattering at (0.5, 0, 0) is centred at $\varepsilon = 0$, and so does not arise from a propagating mode, but is also diffuse in energy and therefore has a finite lifetime. (The intensity centred at $\varepsilon = 0$, increasing as h approaches unity is due to FM fluctuations with maximum at (1, 0, 0)). Warming to 275 K (figure 1(d)) broadens the scattering in both h and ε, that is, it reduces the correlation length and time, but the correlations remain clearly visible. Maps of intensity as a function of energy and momentum along *(h,h,0)* were gathered in parallel, and show little momentum dependence, except for that arising from the FM fluctuations, as is evident from figure 1(g). In particular, there is no AF scattering at (0.5,0.5,0). These data were subsequently subtracted as estimates of the non-magnetic scattering that arises from the sample and cryostat. Figures 1(e) and 1(f) show the energy-integrated scattering at similar temperatures arising from the structural distortions produced by the polarons. The strain field from individual polarons is responsible for the scattering centred at the (2,0,0) Bragg position (Huang scattering), whereas the polaron correlations produce the peaks at $(2+\delta, 0, \pm 1)$, $\delta = 0.275$, an incommensurability reduced from $\delta = 0.30$ for $x = 0.4$ [20]. Just as for the AF fluctuations, warming to 250 K broadens and reduces the intensity of the peaks. (Note that symmetry equivalent scattering at $(2-\delta, 0, \pm 1)$ is largely obscured by scattering from the polycrystalline material of the sample holder and cryostat.) Qualitatively identical intensity maps of scattering from both AF and polaron correlations were gathered from the single crystal with $x = 0.30$, except that the onset of scattering is at $T_N = 90$K, and there is a further reduction of the incommensurate wavevector to $\delta = 0.25$. Figure 4 shows data as a function of δh along $(2+\delta h, 0, 1)$ for both $x = 0.35$ and $x = 0.30$ just above the respective ordering temperatures that show the reduction in δ on reducing x. The data for both hole concentrations are strongly reminiscent of those for $x = 0.40$ for the AF fluctuations [19] and polarons [20].

Quantitative analysis of the intensities is presented in figures 2 and 3. First, let us consider the AF fluctuations. Figure 2(c) shows the integrated intensity for $x = 0.35$. With no applied magnetic field, the intensity increases sharply on warming to a maximum at T_C (as revealed by a comparison with the (004) Bragg peak intensity, which is proportional to the square of the magnetic order parameter, shown in figure 2(a)), and falls only slowly as the temperature is raised further. We confirmed that the AF fluctuations are independent of thermal history

i.e. whether they were collected on warming or cooling through the transition temperature. The intensity tracks that of log(ρ_{ab}) and log(ρ_c). This behaviour is similar to that reported in our earlier work for x = 0.40 [19]. What is additionally revealed is that the AF fluctuations are suppressed in an applied magnetic field of 7 T for temperatures below ~ 200 K, again mimicking the behaviour of log(ρ_{ab}) and log(ρ_c). The same is true for the scans as a function of applied field just above T_C (figures 2(e) and 2(f)). The direct relationship between the intensity of the AF fluctuations and log(ρ_{ab}) is made clear in figure 5, where the temperature and magnetic field dependent AF intensity data of figures 2(c) and 2(f) are plotted as a function of log(ρ_{ab}). Figure 5 shows that there is strong correlation between the intensity of the AF fluctuations and the in-plane resistivity that applies irrespective of the temperature or magnetic field. Similar data is presented for x = 0.30 in figures 3(b) and 3(c). As for x=0.35, the AF fluctuations are independent of warming or cooling through T_N. Two important points emerge from the data for x = 0.30. Firstly, the AF intensity reaches it maximum close to T_N = 90 K, which is substantially less than the temperature of the peak intensity for x = 0.35, which is close to T_C = 121 K. The fact that the peak intensity coincides with the three-dimensional ordering temperature for x = 0.30, 0.35 as well as for 0.40 [19] demonstrates that the phenomenon of AF fluctuations is an intrinsic property of the bilayer manganites, and does not originate from an extrinsic impurity phase. Secondly, the intensity tracks ρ_c, not ρ_{ab}. Note that the AF fluctuations described here are short-range correlations within the bilayers and are unrelated to the critical scattering that is expected near T_N associated the three-dimensional long-range antiferromagnetic order from the antiferromagnetic stacking of the (ferromagnetic) bilayers. That critical scattering is expected at wave vectors (h, k, l) near integer h and k for odd-integer l. The AF fluctuations investigated here are centred on (0.5, 0, 0); nor do their correlation lengths and lifetimes diverge at T_N, as is described below.

The correlation lengths, $\xi = 1/\kappa$, and the inverse lifetimes, $\gamma = 1/\tau$, of the fluctuations as a function of temperature in zero applied field for both x=0.30 and x=0.35 are shown in figures 6(c) and 6(d). They were obtained from fits to sections parallel to the $(h,0,0)$ and ε axes from the momentum and energy intensity maps, of which figures 6(a) and 6(b) are examples taken from the maps in figures 1(c) and 1(d). The momentum and energy dependence of the AF fluctuations was modelled by the following function:

$$A\,|F(|\boldsymbol{Q}|)|^2\,\frac{\exp\left(-\left(q_{ip}/\kappa\right)^2\ln 2\right)}{\kappa^2}\,\frac{\varepsilon}{1-\exp\left(-\varepsilon/k_BT\right)}\,\frac{\gamma/\pi}{\varepsilon^2+\gamma^2}\cos^2\left(Q_z a/2\right)$$

where κ, γ and the overall scale factor, A, were treated as free parameters to be obtained from simultaneous least-squares fitting of the model to the pair of sections for each temperature. In the model, $\boldsymbol{Q}$ is the momentum with Q_z the component (in Å^{-1}) along the direction perpendicular to the plane of the bilayers, q_{ip} is the in-plane momentum (in Å^{-1}) with respect to the origin of the AF fluctuations at (0.5,0,0), a = 3.87 Å is the Mn-Mn distance within a bilayer, $|F(|\boldsymbol{Q}|)|^2$ is the magnetic form factor for Mn^{3+}, and $1/\left(1-\exp\left(-\varepsilon/k_BT\right)\right)$ is the detailed balance factor. The more conventional Lorentzian form for momentum correlations, $1/\left(\kappa^2+q_{ip}^2\right)$, has been replaced by a Gaussian with the same height and half-width half-maximum to make the determination of κ less sensitive to details of the tails of the momentum correlation function. The non-linear tail from the FM fluctuations centred on (1,0,0) was accounted for by a Gaussian function in momentum. The cosine-squared modulation of intensity perpendicular to the bilayers arises from FM correlation of the moments along Mn-Mn bonds connecting the two sheets of the bilayer. This variation with Q_z was measured for both x = 0.30 and 0.35, and together with the absence of magnetic scattering at (0.5,0.5,0) confirms that the instantaneous ordering wavevector in the AF correlated regions is the same as that found for x = 0.40 [19] and shown in figure 1(b). For both x = 0.30 and 0.35, ξ and γ are almost identical, as is shown in figures 6(c) and 6(d), varying according to temperature between 1 - 2 Mn-Mn distances and 0.5 – 4 meV ($\equiv \tau \sim 1$ – 0.1 ps), values very similar to those for x = 0.40. Both ξ and γ show no evidence of divergence near the critical temperature, but instead vary slowly and monotonically on warming through T_N (x = 0.30) or T_C (x = 0.35). This result, in conjunction with the temperature dependence of the intensity of the AF scattering, implies that near the critical temperature the volume fraction of AF correlated regions is changing, but that the size and longevity of the regions themselves does not change.

We turn now to the polaron correlations. Figures 2(d) and 3(d) show the temperature variation of the scattering intensity for x = 0.30 and x = 0.35 respectively. With no applied magnetic field, the intensity appears rapidly on warming through the critical temperature, with the peak close to T_N (x = 0.30) or T_C (x = 0.35), and decreasing slowly as the temperature is raised further. This behaviour is qualitatively the same as that of the AF

fluctuations. The intensity is similarly suppressed by the application of a 7 T magnetic field (also figures 2(d) and 3(d)). In the case of $x = 0.35$, we also performed a scan as a function of applied field at 135 K = T_C +14 K, which, just like the AF intensity, tracks the field dependence of ρ_{ab} (figures 2(e) and 2(g)) [26].

4. Discussion

Our results can be summarised as follows: (i) short-range (~2 *a*), short-lived ($\gamma \sim 0.5 - 4$ meV) AF correlations are a common feature in the bilayer manganites $La_{2-2x}Sr_{1+2x}Mn_2O_7$, $x = 0.30 - 0.40$, which appear on warming above the three-dimensional magnetic ordering temperature; (ii) the intensity of the correlations tracks the resistivity both as a function of temperature and applied magnetic field; (iii) on cooling through T_N or T_C the population of AF correlated regions collapses, but the nature of the regions, as characterised by their extent and lifetime, does not change; (iv) correlated polarons appear above T_N ($x = 0.30$) or T_C ($x = 0.35$), whose temperature and magnetic field dependent scattering intensity likewise tracks that of the resistivity. The association of both phenomena to the resistivity suggests a close relation which proceeds via Anderson localisation, as described in our original paper [19].

One possibility is that the AF fluctuations (AFF) follow from the atomic arrangements associated with the polaron correlations (PC). Both break the tetragonal symmetry by selecting one of the in-plane Mn-Mn directions, the former selecting the direction for AF correlations of Mn moments, and the latter selecting the direction for modulated elongation of the Mn-Mn octahedra [21]. However, the wavevectors are different, at 0.5 (AFF) and $\delta = 0.25 - 0.30$ (PC), but these are not serious discrepancies given that the correlation lengths, $< 2\ a$ for the AFF, and ≈ 5-6 *a* for the polarons, are of the same order as the periodicities implied by the wavevectors at which the fluctuations are peaked. Weak modulation of the FM bonds along *(h, 0, 0)* from modulation of the occupancy of the $3x^2$-r^2 orbital [21, 22] would result in ferrimagnetic correlations. Alternatively, sufficiently large modulation of the charge ordering allows for AF interactions along (h, 0, 0) between Mn sites that bracket the valence maxima in the charge modulation (due to superexchange between the t_{2g} electrons), and/or AF interactions along (0, k, 0) at the valence minima (from application

of the Goodenough-Kanamori rules for the sign of magnetic exchange integrals in charge-ordered transition metal oxides [27, 28]).

In the above we have presupposed that the charge and lattice distortions are static and thereby set the stage for the AF fluctuations. This is actually erroneous because the timescales for the AF and correlated polaron fluctuation are comparable: the lifetimes of the AF fluctuations at T_N ($x = 0.30$) or T_C ($x = 0.35$) are $\tau \approx 2$ ps and ≈ 1 ps respectively ($\equiv \gamma \approx 0.6 - 1.0$ meV), while the characteristic timescale quoted for the polaron correlations for x = 0.40 is ~1 ps [20]. The consequence is that the dynamic objects responsible for both the AFF and PC's must be thought of as either the same bubbles or co-existing bubbles nucleating, decaying and moving in the MnO planes which are interleaved with the chemically disordered (La,Sr)O planes. The underlying Born-Oppenheimer approximation notwithstanding, the previous paragraph provides a starting point for a description where the largest lattice distortions coincide with antiferromagnetism, resulting in single bubbles.

An alternative possibility to that of the AF fluctuations occurring within regions of correlated polarons is that they are separate phenomena – for example the AF correlations could be found at the boundaries between nanodomains of correlated polarons with average size $\xi \sim 6a$. Nanoscale inhomegeneity in the manganites is a common phenomenon both experimentally and theoretically [14]. The coexistence of AF and FM fluctuations above T_C for $x = 0.40$ has already been explained as arising from different but adjacent nanovolumes defined by the static (on the scale of the underlying hopping matrix elements) disorder potential [19] (see also [29, 30]). In cuprates, phenomena belonging to different co-existing nearly macroscopic sub-volumes have been observed, for example spatial exclusivity between polarons and oxygen ordering in oxygen over-doped La_2CuO_{4+y} [31].

There is little qualitative difference in the AF fluctuations and polaron correlations measured for the three compositions $x = 0.40$, 0.35 and 0.30. On the other hand, the $x = 0.30$ material stands out, as do the superconducting cuprates, in displaying metallic (i.e. resistivity decreasing with T) transport within the bilayers above the ordering temperature even while the interlayer transport is that of an insulator [18]. The analogy with the cuprates is complete also below the ordering temperature in the sense that the $x = 0.30$ manganite becomes (except at the lowest fields and temperatures) a three-dimensional metal and the cuprates become three-dimensional superconductors. From scanning tunnelling microscopy and infrared spectroscopy for $x = 0.30$, the out-of-plane resistivity as a function of temperature was

explained by confinement of mobile polarons within the two-dimensional bilayer sheets, with hopping between the bilayers requiring their costly deconstruction and reconstruction [32]. In the language of the localisation problem, the slow fluctuations (seen by magnetic and non-magnetic neutron scattering as in this paper) in the potential sensed by the polarons formed around the holes are relatively small on the scale of their effective in-plane hopping t_{ab}^{eff} and large on the scale of the interbilayer t_c^{eff} . Thus, in the high temperature phase, the relation between the scattering data and electrical transport suggested by strong localisation will obtain for ρ_c but not ρ_{ab}. As the Fermi level and effective hopping terms are changed, for example by increasing the composition x from 0.30, both t_{ab}^{eff} and t_c^{eff} can become sufficiently small to confine the motion of the holes in *all three* dimensions, implying that ρ_{ab} as well as ρ_c will track the measured scattering intensities in similar ways. Of course, ferromagnetic ordering, induced by cooling and/or magnetic fields, will - on account of the double exchange mechanism - enhance the effective hopping so as to defeat Anderson localization in all three dimensions, leaving only relatively subtle interlayer tunnelling and weak localization effects to dominate at low temperatures and fields.

5. Conclusion

We have shown that the appearance of short-range, short-lived, AF fluctuations on warming into the paramagnetic phase is a common feature of the bilayered manganites $La_{2-2x}Sr_{1+2x}Mn_2O_7$, $x = 0.30 – 0.40$. The dependency of the intensity of the AF fluctuations on both temperature and applied magnetic field closely follows that of ρ_{ab} and ρ_c for $x = 0.35$, and ρ_c for $x = 0.30$. The intensity of the polaron correlations that appear on warming into the paramagnetic phase also tracks the temperature and magnetic field dependent resistivity. The possible relationship of the AF and polaron correlations, implied by their association with the resistivity, is discussed. The observed interplay of static chemical disorder, lattice dynamics and spin fluctuations presents the type of puzzle which we would have very much enjoyed to present to Roger Cowley, and which we now offer in his memory.

References

[1] R.A. Cowley, Phys. Rev. **134** A981 (1964).
[2] R.A. Cowley et al., Phys. Rev. B **15** 4292 (1977).
[3] R.J. Birgeneau et al., Phys Rev B **21** 317 (1980).
[4] R.J. Birgeneau et al., Phys. Rev. B **21** 4038 (1980).
[5] H. Yoshizawa et al., Phys. Rev. Lett. **48** 438 (1982).
[6] R.J. Birgeneau et al., Phys. Rev. B **28** 1438 (1983).
[7] D.A. Tennant et al., Phys. Rev. Lett. **70** 4003 (1993).
[8] P.W. Anderson and H.Hasegawa, Phys.Rev. **100** 67 (1955).
[9] A. Millis, Nature **392** 147 (1998) and references therein.
[10] H. Kuwahara et al., Science **270** 961 (1995).
[11] A. Asamitsu et al., Nature **388** 50 (1997).
[12] K. Miyano et al., Phys. Rev. Lett. **78** 4257 (1997).
[13] J-S. Zhou et al., Phys. Rev. Lett. **79** 3234 (1997).
[14] E. Dagotto et al., Phys. Rep. **334** 1-153 (2001) and references therein.
[15] Ch. Renner et al., Nature **416** 520 (2002).
[16] L. Zhang et al., Science **298** 805 (2002).
[17] Y. Moritomo et al., Nature **380** 141 (1996).
[18] T. Kimura et al., Science **274** 1698 (1996).
[19] T.G. Perring et al., Phys. Rev. Lett. **78** 3197 (1997).
[20] L. Vasiliu-Doloc et al. Phys. Rev. Lett. **83** 4393 (1999).
[21] B.J. Campbell et al., Phys. Rev. B **65** 014427 (2001).
[22] B.J. Campbell et al., Phys. Rev. B **67** 020409 (2003).
[23] M. Kubota et al., J. Phys. Soc. Jpn. **69** 1986 (2000). This paper also mentions that polaron correlations exist for $0.30 \leq x < 0.4$ with smaller δ, but presents no data and is otherwise concerned exclusively with $x = 0.40 – 0.48$.
[24] M. Kubota et al., J. Phys. Chem. Solids **60** 1161 (1999).
[25] M. Kubota et al., Phys. Rev. Lett. **91** 047201 (2003).
[26] The magnetic field dependency of the polaron correlation peak at (2.3,0,1) for $x = 0.40$ is reported in [20]. It almost disappears by 1T, in contrast to our results for $x = 0.30$ and $x = 0.35$. This may be due to different analysis methods. In Ref. [20] the peak arising from the correlated polarons was isolated from the tail of the Huang scattering by fitting the data to a non-linear 'background'. In the present case, the full diffuse scattering signal in the range $2.12 \leq h \leq 2.37$ (x=0.30) $2.15 \leq h \leq 2.40$ (x=0.35) was integrated.
[27] J.B. Goodenough, Phys. Rev. **100** 564 (1955).
[28] J. Kanamori, J. Phys. Chem. Solids **10** 87 (1959).
[29] A. J. Millis, Phys. Rev. Lett. **80** 4358 (1998).
[30] T.G. Perring et al., Phys. Rev. Lett. **80** 4359 (1998).
[31] N. Poccia et al., Proc. Natl. Acad. Sci. **109** 15690 (2012).
[32] H.M. Rønnow et al., Nature **440** 1025 (2006).
[33] T.G. Perring et al., Phys. Rev. B **58** R14693 (1998).

Figure Captions

Figure 1. Crystal structure of $La_{2-2x}Sr_{1+2x}Mn_2O_7$, and scattering intensity maps of the AF fluctuations and polaron correlations for $x = 0.35$, at temperatures just above $T_C \equiv 121$ K, and close to room temperature. (a) MnO_6 octahedra are shown in orange; the green circles correspond to La and Sr. (b) The local, instantaneous, arrangement of magnetic moments in the antiferromagnetically correlated regions in a bilayer. Note that the data determine the antiferromagnetic ordering wave vector, but not the direction of the magnetic moments; they are drawn in-plane here but could equally be perpendicular to the plane of the bilayers as was drawn in figure 1(c) of [19]. (c) The spectrum of the magnetic fluctuations as a function of energy, ε, and momentum along *(h, 0, 0)* at 125K and (d) 275K, showing the short-range, short-lived AF fluctuations centred at $h = 0.5$ and zero energy. The spectra were determined by taking the difference between the measured intensity maps along the *(h, 0, 0)* and *(h, h, 0)* directions, collected in parallel in different detector banks of the HET spectrometer. Except close to (000), the intensity along *(h, h, 0)* is almost independent of momentum, and arises from non-magnetic scattering by the sample and container. (e) Energy-integrated scattering (the spectrum of the moderator used peaks at ≈10 meV) taken on the PRISMA diffractometer as a function of momentum in the *(h, 0, l)* plane for 135K and (f) 250K, determined by taking the difference between the measured intensities at those temperatures and that at 10K ($<< T_C$), the lowest temperature measured. The scattering from polaron correlations is centred at (~2.3,0,±1), and the Huang scattering is centred around (200). The arcs of intensity centred on (000) arise from powder diffraction from the aluminium sample holder and heat shields on the cryogenic equipment. The incomplete subtraction of the arcs is due to changes in the Debye-Waller thermal factor, as is that at the (200) and (202) Bragg positions. (g) Map of scattering intensity in the *(h, k, 0)* plane integrated over the energy range $-5 \le \varepsilon \le 5$ meV for T = 126K. The non-magnetic scattering and background has been removed by subtracting data collected at 6K ($<< T_C$).

Figure 2. Summary of magnetic and polaron scattering intensities, and resistivity, for $x = 0.35$: (a) Magnetic order parameter squared for $x = 0.35$ as determined by the (004) Bragg peak intensity. The almost constant value at $T >$ ~120K arises from the structural (i.e. non-magnetic) Bragg peak. (b) In-plane and out-of-plane resistivities, ρ_{ab} and ρ_c, at 0 T and 7 T.

(c) Magnetic scattering centred on the AF reciprocal lattice position as a function of temperature, obtained by integrating the measured energy-momentum intensity maps over $0.35 \leq h \leq 0.65$ and $-15 \leq \varepsilon \leq 15$, and subtracting the lowest temperature at which data were gathered, which arises solely from non-magnetic scattering from the sample and cryogenic equipment. (d) Intensity of the energy-integrated scattering from polaron correlations around $(2+\delta, 0, \pm 1)$, $\delta = 0.275$, as a function of temperature, obtained by taking the section $2.15 \leq h \leq 2.40$ from the intensity maps in the $(h, 0, l)$ plane, fitting the resulting function of l to a pair of peaks centred at $l \approx \pm 1$ on a linear background, and adding the two peak areas. (e) ρ_{ab} and ρ_c, (f) magnetic scattering and (g) scattering from polaron correlations, as a function of applied magnetic field.

Figure 3. Summary of magnetic and polaron scattering intensities, and resistivity, for $x = 0.30$: (a) Magnetic order parameter squared for $x = 0.30$ as determined by the (005) magnetic Bragg peak intensity. The unusual shape is due to the fact that the spins rotate from perpendicular to the plane of the bilayers for $T << T_N$ to lying within the bilayers as T approaches T_N [33] (b) In-plane and out-of-plane resistivities, ρ_{ab} and ρ_c, at 0 T and 7 T. (c) Magnetic scattering centred on the AF scattering position as a function of temperature, obtained by the same procedure as for $x = 0.35$ described in the caption for figure 2(c). (d) Intensity of the energy-integrated scattering from polaron correlations around $(2+\delta, 0, \pm 1)$, $\delta = 0.25$, as a function of temperature, obtained by the same procedure as for x = 0.35 described in the caption for figure 2(d), except that $2.12 \leq h \leq 2.37$.

Figure 4. Cuts as a function δh in $(2+\delta h, 0, 1)$ through the polaron correlation peaks at $(2+\delta, 0, 1)$ to determine the incommensurate ordering wavevector, δ, (a) for $x = 0.35$ ($T = 135$ K), showing $\delta = 0.275$, and (b) for x = 0.30 ($T = 100$ K), showing $\delta = 0.25$.

Figure 5. Intensity of the AF fluctuations as a function of $\log(\rho_{ab})$. The 0T data, 7T and field-scan data taken at 127K, taken from figure 2(c) and figure 2(f), are indicated by the blue, red

and yellow symbols respectively. The line is the result of a linear regression to the data points.

Figure 6. (a) Sections from the intensity maps gathered for $x = 0.35$ in figure 1(c) and figure 1(d) as a function of ε integrated over $0.35 \leq h \leq 0.65$, and (b) as a function of h integrated over $-5 \leq \varepsilon \leq 5$. The lines show the result of fits to the model described in the text. (c) Correlation length ξ, and (d) inverse lifetime $\gamma \equiv 1/\tau$ for $x = 0.35$ (circles, blue) and $x = 0.30$ (triangles, red). Error bars are smaller than the symbols except where shown.

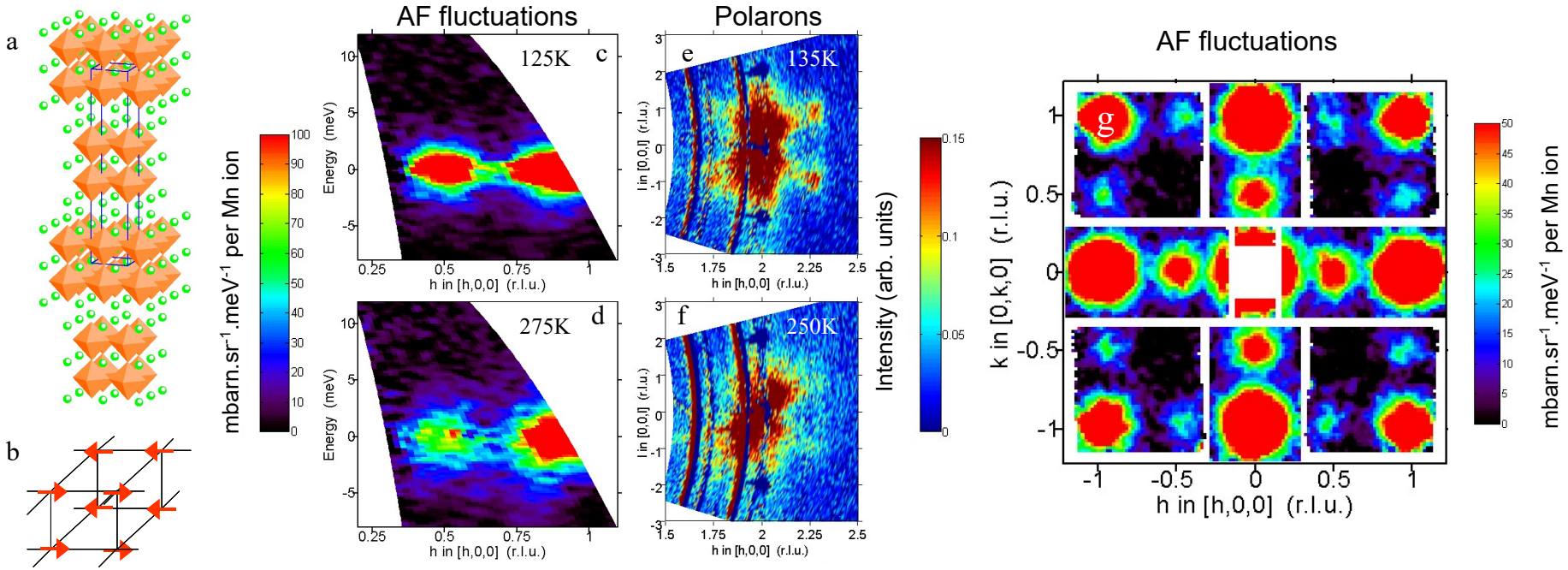

Figure 1 (Perring et. al.)

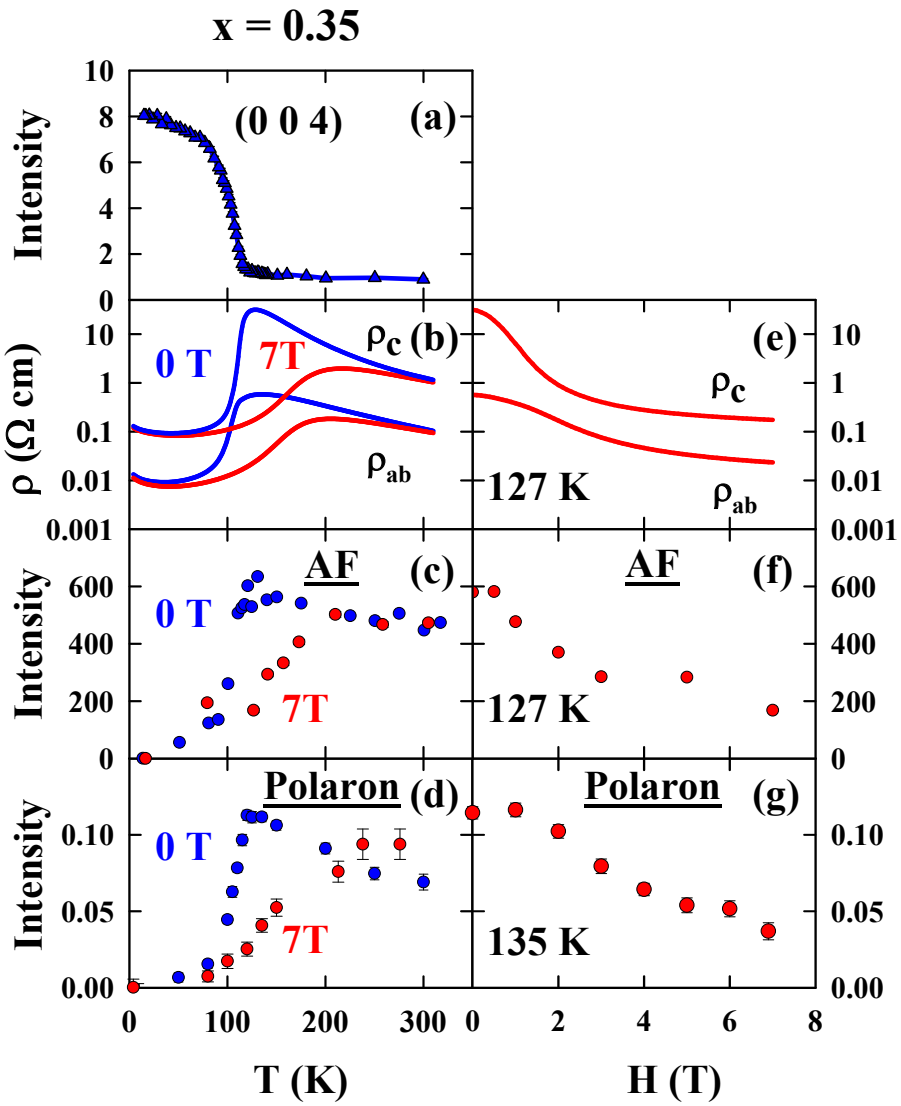

Figure 2 (Perring et. al.)

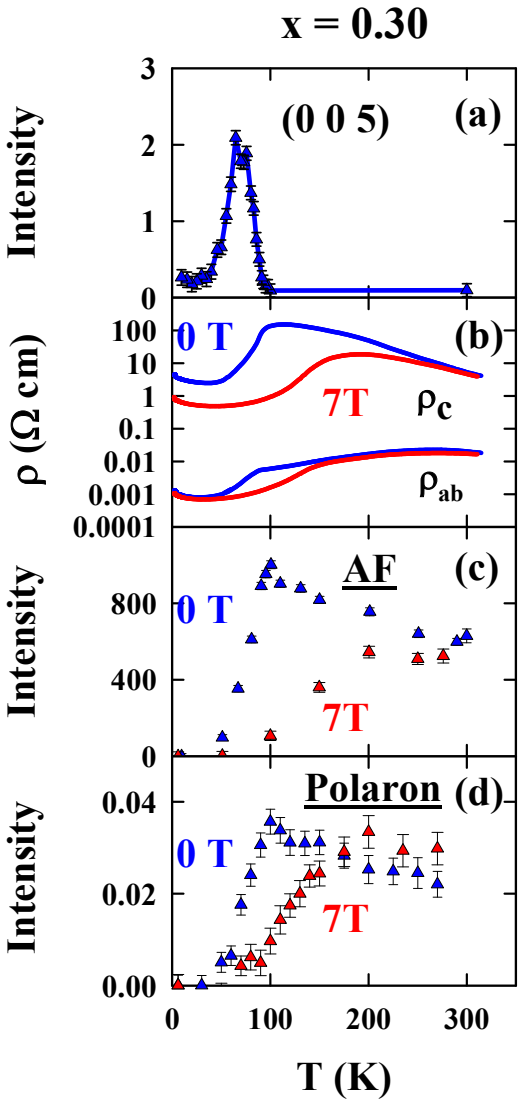

Figure 3 (Perring et. al.)

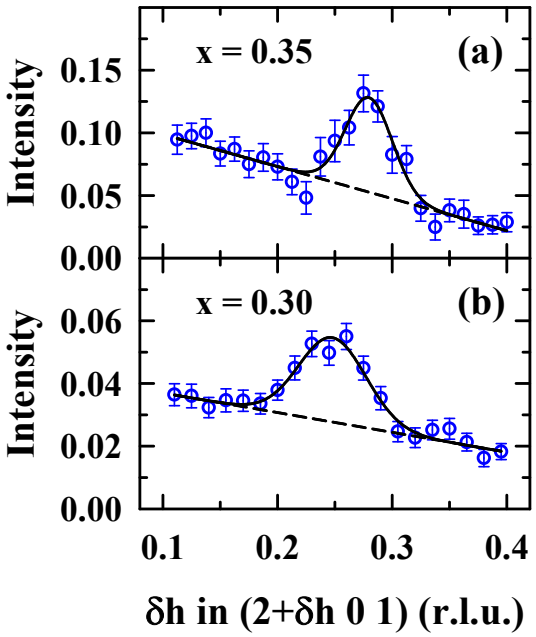

Figure 4 (Perring et. al.)

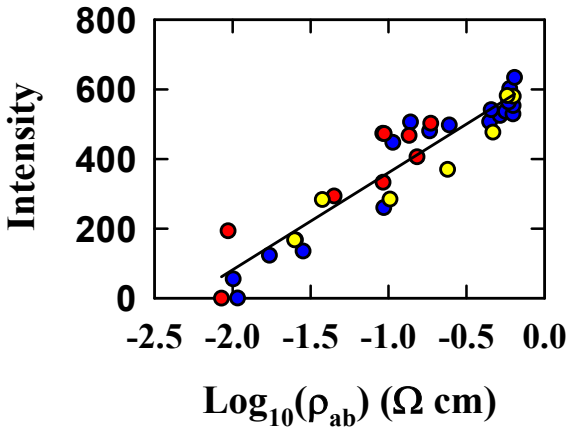

Figure 5 (Perring et. al.)

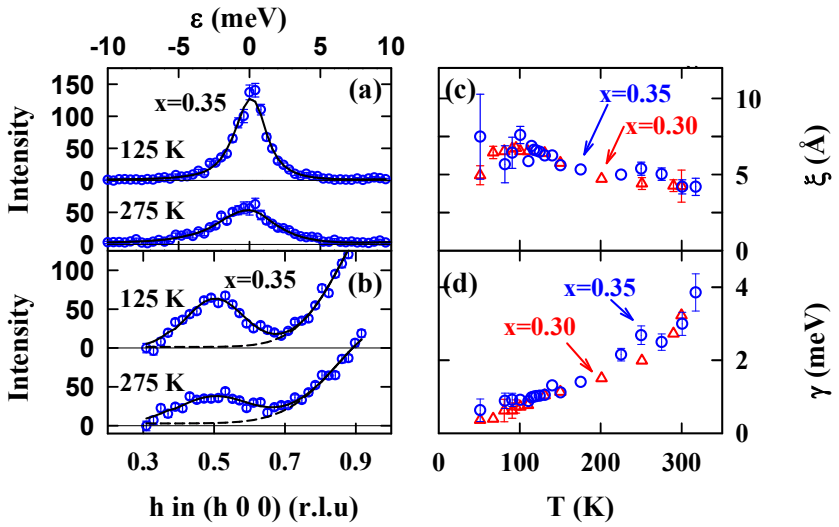

Figure 6 (Perring et. al.)